transmit-receive mode) or by a separate detector coil or coils. Images are reconstructed from the acquired data by Fourier transformation. Here, sagittal images (i.e., in a vertical plane parallel to the bore of the magnet) were acquired using a standard spin-echo sequence, in which after the exciting pulse a further RF pulse refocuses the signal to form an "echo." Because only part of the data is acquired at any one excitation, the process is repeated and a time period (the repeat time or *TR*) is allowed between excitations to allow for the recovery of the magnetization. In this study, *TR* was 400 ms and the echo time (*TE*) was 15 ms. The FOV was 300 mm by 300 mm with a 256×128 data matrix reconstructed to a 256×256 image matrix. A single acquisition with no averaging was used in all cases.

The first image (Fig. 4B) was obtained using the "body coil" in transmit-receive mode. This procedure allowed the precise position of the thumb to be determined, so that the subsequent images could be set up accurately. Despite using increased gain, no image could be detected with the small coil alone (Fig. 4C). However, when the bundle of 19 Swiss rolls, 200 mm long, was used to couple the thumb to the receiver coil, a clear image of the thumb was seen (Fig. 4D).

Note that the body coil image (Fig. 4B) allows visualization of the full thumb. This is because the whole of the thumb (and, indeed, beyond) was excited by the RF pulses, and hence was emitting signals. The image obtained by flux guidance through the Swiss rolls is limited by the spatial extent of the flux that could be collected (Fig. 4D). The ratio of the signal measured in a region of the thumb located centrally (10 mm above the free surface of the flux guide) to that measured in a similar region of interest placed in air gave a signal-to-noise ratio (SNR) of 32 for the solenoid with Swiss rolls. The precise SNR value achieved is strongly dependent on the details of measurement because of the spatial nonuniformity of the sensitivity pattern, and it is also dependent on the coupling between the flux guides and the receiver coil. Without the Swiss rolls, no signal from the thumb was detectable with the solenoid coil.

The presence of the Swiss rolls introduces negligible distortion of the main field or the field gradients B_0, because the material has a relative permeability close to unity at dc. Nor does it noticeably distort the effect of the RF excitation field B_1. The spin excitation produced by B_1 is determined by its time integral. Because the material is highly anisotropic, it only interacts with B_1, which is a rotating field, over a very small angular range. Even strong interactions result in only slight perturbations in response, provided they only occur over a small fraction of each cycle, as in this case.

We have demonstrated the unique properties of a microstructured magnetic material operating in the RF band. The material offers a range of frequency-specific permeabilities that can differ widely from unity. The material was used here in an MRI machine to guide the RF flux from an object to a remote receiver coil with little flux leakage, although the material itself was not optimal. In effect, the material has potential to change approaches to optimizing the coil filling factor in nuclear magnetic resonance systems in general, and MRI scanners in particular (*15, 16*). Improved material should allow much better noise performance, and we expect this to have a substantial impact on the RF systems used in MRI equipment. Finally, we note that the characteristics shown in Fig. 2 indicate that there are frequencies at which $\mu = 0$, when the material would act as a screen, and further frequencies where μ is negative, leading to other unique capabilities. Exploiting this class of materials could fundamentally change existing approaches to magnetic resonance imaging and spectroscopy.

References and Notes

1. H. Ghiradella, *Appl. Opt.* **30**, 3492 (1991).
2. E. Yablonovitch, *Phys. Rev. Lett.* **58**, 2059 (1987).
3. S. John, *Phys. Rev. Lett.* **59**, 2486 (1987).
4. K. M. Ho, C. T. Chan, C. M. Soukoulis, *Phys. Rev. Lett.* **65**, 3152 (1990).
5. E. Yablonovitch, T. J. Gmitter, K. M. Leung, *Phys. Rev. Lett.* **67**, 2295 (1991).
6. D. F. Sievenpiper, M. E. Sickmiller, E. Yablonovitch, *Phys. Rev. Lett.* **76**, 2480 (1996).
7. J. B. Pendry, A. J. Holden, W. J. Stewart, I. Youngs, *Phys. Rev. Lett.* **76**, 4773 (1996).
8. J. B. Pendry, A. J. Holden, D. J. Robbins, W. J. Stewart, *J. Phys. Condens. Matter* **10**, 4785 (1998).
9. D. F. Sievenpiper, L. Zhang, R. F. J. Broas, N. G. Alexopolous, E. Yablonovitch, *IEEE Trans. Microwave Theory Tech.* **47**, 2059 (1999).
10. J. B. Pendry, A. J. Holden, D. J. Robbins, W. J. Stewart, *IEEE Trans. Microwave Theory Tech.* **47**, 2075 (1999).
11. D. R. Smith, W. J. Padilla, D. C. Vier, S. C. Nemat-Nasser, S. Schultz, *Phys. Rev. Lett.* **84**, 4184 (2000).
12. V. G. Veselago, *Sov. Phys. Uspekhi* **10**, 509 (1968).
13. ProFilm material (otherwise known as Oracover) is manufactured by Lanitz-Prena Folien Factory GmbH, Leipzig, and distributed by J. Perkins Distributors Ltd., London.
14. J. A. Stratton, *Electromagnetic Theory* (McGraw-Hill, New York, 1941), pp. 211–214.
15. D. I. Hoult, R. E. Richards, *J. Magn. Reson.* **24**, 71 (1976).
16. D. I. Hoult, P. C. Lauterbur, *J. Magn. Reson.* **34**, 425 (1979).

17. I.R.Y., D.J.L., D.J.G., and J.V.H. are grateful to Marconi Medical Systems for substantial financial support of the work at the Robert Steiner Magnetic Resonance Unit.

16 October 2000; accepted 20 December 2000

Functional Nanoscale Electronic Devices Assembled Using Silicon Nanowire Building Blocks

Yi Cui[1] and Charles M. Lieber[1,2]*

Because semiconductor nanowires can transport electrons and holes, they could function as building blocks for nanoscale electronics assembled without the need for complex and costly fabrication facilities. Boron- and phosphorous-doped silicon nanowires were used as building blocks to assemble three types of semiconductor nanodevices. Passive diode structures consisting of crossed *p*- and *n*-type nanowires exhibit rectifying transport similar to planar *p-n* junctions. Active bipolar transistors, consisting of heavily and lightly *n*-doped nanowires crossing a common *p*-type wire base, exhibit common base and emitter current gains as large as 0.94 and 16, respectively. In addition, *p*- and *n*-type nanowires have been used to assemble complementary inverter-like structures. The facile assembly of key electronic device elements from well-defined nanoscale building blocks may represent a step toward a "bottom-up" paradigm for electronics manufacturing.

Miniaturization of silicon electronics is being intensely pursued (*1*), although fundamental limits of lithography may prevent current techniques from reaching the deep nanometer regime for highly integrated devices (*2*). The use of nanoscale structures as building blocks for self-assembled (*3–6*) structures could potentially eliminate conventional and costly fabrication lines, while still maintaining some concepts that have proven successful in microelectronics. One-dimensional structures, such as nanowires (NWs) and carbon nanotubes (NTs), could be ideal building blocks for nanoelectronics (*7, 8*), because they can

[1]Department of Chemistry and Chemical Biology and [2]Division of Engineering and Applied Sciences, Harvard University, Cambridge, MA 02138, USA.

*To whom correspondence should be addressed. E-mail: cml@cmliris.harvard.edu

function both as devices and as the wires that access them. Electrical transport studies of NTs have yielded data supporting the possibility of field-effect transistors (*9, 10*), low-temperature single-electron transistors (*11, 12*), intramolecular metal-semiconductor diodes (*13, 14*), and intermolecular-crossed NT-NT diodes (*15*). However, the use of NT building blocks is limited, because the selective growth and/or assembly of semiconducting or metallic NTs (*7, 8*) is not currently possible.

Successful implementation of a building-block approach for the assembly of nanodevices and device arrays will require that the electronic properties of the blocks be defined and controlled. Recently, we demonstrated that the carrier type (electrons, *n*-type; holes, *p*-type) and carrier concentration in single-crystal silicon NWs (SiNWs) could be controlled during growth, using phosphorous and boron dopants (*16*). We now report the rational assembly of these well-defined SiNW building blocks into functional electronic devices in which critical junctions are formed by the assembly of one or more SiNW/SiNW crosses using *p*- and *n*-type materials.

The *n*- and *p*-type SiNWs were synthesized by laser-assisted catalytic growth (*16*). Different junctions (e.g., *n-n*, *p-p*, and *p-n*) were formed by sequential deposition of solutions of *n*- and *p*-type materials or by manipulation, and contacts to the SiNWs were defined by electron beam lithography (*16, 17*). Field emission scanning electron microscopy (FESEM) was used to image a typical *p-n* junction assembled from 20-nm-diameter *p*- and *n*-type SiNWs (Fig. 1A). Current versus voltage (*I-V*) data recorded on the individual *p*- and *n*-type SiNWs (Fig. 1B) are linear and indicate that metal-SiNW contacts are ohmic (*18, 19*), and thus will not make a significant contribution to the *I-V* behavior of the junctions. Significantly, four-terminal *I-V* measurements made on the *p-n* junction formed at the NW-NW cross show good current rectification (Fig. 1B). These nanoscale junctions thus exhibit similar behavior to bulk semiconductor *p-n* junctions.

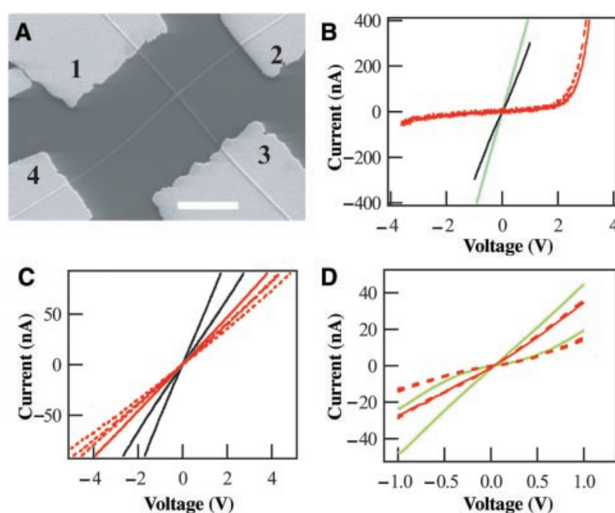

Fig. 1. Crossed SiNW junctions. (**A**) Typical FESEM image of a crossed SiNW junction with Al/Au contacts. The scale bar is 2 μm. The diameters of the NWs used in these studies ranged from 20 to 50 nm. (**B** through **D**) *I-V* behavior of *p-n*, *p-p*, and *n-n* junctions, respectively. The black and green curves correspond to the *I-V* behavior of individual *p*- and *n*-type SiNWs, respectively. The red curves represent *I-V* behavior of junctions. (B) The red curves correspond to four-terminal *I-V* through the *p-n* junction; the current values are multiplied by 10. The solid line corresponds to voltage drop measured between leads 3 and 4, and the dashed line to voltage between 3 and 2. (C and D) The red curves are two-terminal *I-V* through *p-p* and *n-n* junctions, respectively. The solid lines correspond to data from contacts 1-2, and the dashed lines correspond to data from the other three pairs (that is, 1 and 4, 2 and 3, and 3 and 4).

Current rectification has been observed in more than 40 *p-n* junctions assembled from SiNWs in the cross geometry and, we believe, is a robust phenomenon for these NW junction structures. We carried out additional experiments to demonstrate that this diode behavior is indeed due to the *p-n* junction formed by the *p*- and *n*-type SiNWs. First, four-terminal *p-n* junction transport measurements made through different combinations of the contacts show similar rectifying behavior and current level (solid and dashed curves, respectively; Fig. 1B), are similar to two-terminal junction measurements, and show that current is substantially smaller than that through the individual SiNWs, demonstrating that the junction dominates the *I-V* behavior. Second, transport data recorded on *p-p* (Fig. 1C) and *n-n* (Fig. 1D) junctions show linear or nearly linear behavior, demonstrating that interface oxide between individual SiNWs does not produce a significant tunneling barrier (*20, 21*), as such a barrier would lead to highly nonlinear *I-V*. Hence, our data show that crossed SiNWs make good electrical contact with each other despite the small contact area (10^{-12} to 10^{-10} cm^2) and simple method of junction fabrication, and can exhibit good diode behavior in the case of *p-n* junctions.

Because *p-n* junctions represent the basic element of many devices (*19*), including amplifiers and switches, we have explored the possibility of assembling such devices at the nanometer scale using our *n*- and *p*-type SiNWs. First, the assembly and transport properties of bipolar transistors (*19*), which are active devices capable of current gain, have been investigated. The conventional structure of a bipolar transistor (Fig. 2A, left) requires three distinct material types: for example, a highly doped *n*-type (n^+) layer, which is the emitter (E), a *p*-type base (B), and an *n*-type collector (C). Significantly, this basic n^+-*p*-*n* structure can be easily realized (*22*) by assembling n^+- and *n*-type SiNWs across a *p*-type SiNW base (Fig. 2A, right, and Fig. 2B).

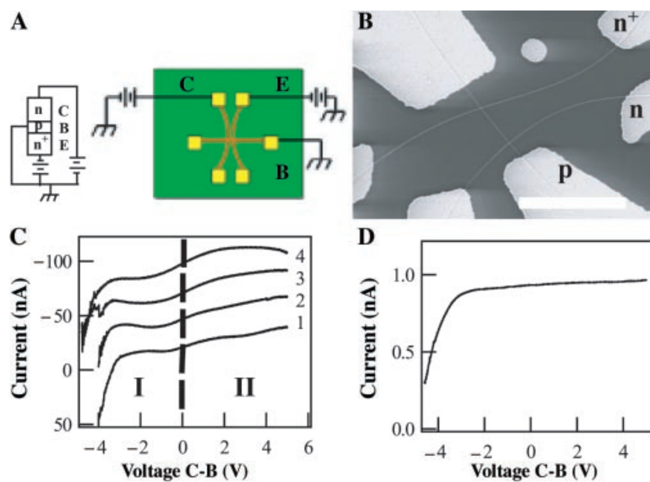

Fig. 2. Shown are n^+-*p*-*n* SiNW bipolar transistors. (**A**) Schematics illustrating the common base configuration of an n^+-*p*-*n* bipolar transistor (*19*) and the corresponding structure built from crossed SiNWs (right). The n^+-, *p*-, and *n*-type SiNWs function as emitter, base, and collector, respectively. (**B**) Typical FESEM image of SiNW bipolar transistor. The three wires labeled as n^+, *p*, and *n* were used as emitter, base, and collector, respectively. Scale bar, 5 μm. (**C**) Collector current versus collector-base voltage recorded on an n^+-*p*-*n* transistor with emitter and collector SiNWs 15 μm apart. Curves 1 to 4 correspond to the data recorded for emitter-base voltages of −1, −2, −3, −4 V, respectively. Regime I and II are separated by a dashed line, corresponding to saturation mode and active mode, respectively. (**D**), The common base current gain versus collector-base voltage.

Transport measurements made on the individual n^+-, *n*-, and *p*-type SiNWs, and the n^+-*p* and *p-n* NW junctions showed that the metal contacts to individual SiNWs were

ohmic or nearly ohmic and that the junctions were rectifying. The behavior of the bipolar transistor was assessed from measurements of the collector current as a function of C-B voltage (Fig. 2C); the n^+-SiNW emitter was set at different forward bias values (curves 1 through 4) for these measurements. In general, the collector current is relatively constant (versus C-B voltage) in region II (Fig. 2), corresponding to the collector in reverse bias with only a very small leakage current, and this current value increases as the emitter forward bias/injected current is increased (*23*). This large flow of collector current in reverse bias demonstrated transistor action. Hence, these simple SiNW-based bipolar transistors exhibit behavior similar to that found in standard planar devices (*19*), and moreover, can exhibit very good current gain.

The common base current gain, defined as the ratio of the collector current to emitter current (Fig. 2D), and corresponding common emitter current gain, defined as the ratio of collector current to base current, have values of 0.94 and 16, respectively. The relatively large current gain observed in these simple devices suggests several important points. First, the efficiency of electron injection from emitter to base must be quite high. We believe that efficiency reflects our ability to control doping in these nanowires and produce the desired n^+-p E-B junction. Second, these relatively large current gains have been achieved in a device (Fig. 2) with a large (15 μm) base width, suggesting that the mobility of injected electrons can be quite high in the SiNWs. These observations also indicate clear directions for improving the SiNW bipolar transistors. For example, it will be interesting to study the current gain as a function of base width, because it is possible to assemble structures with separations of the n^+ and n NWs on the order of 100 nm or less.

We have also carried out preliminary experiments to explore the assembly of other types of devices using these SiNW building blocks. Specifically, the ability to prepare *n*- and *p*-type NWs enables the assembly of complementary inverter-like structures (Fig. 3), which in analogy to conventional Si technology, could exhibit the low static power dissipation critical to highly integrated nanoelectronics. The lightly doped *p*- and *n*-type SiNWs used in the inverters show large gate effects and can be completely depleted (Fig. 3B, inset). The output voltage from the device (V_{out}) varies from negative (high) to zero as the input gate voltage (V_{in}) from positive to negative; that is, the signal is inverted. From the slope of transfer characteristics, we calculate a voltage gain of 0.13. The low gain exhibited by our initial devices could be improved by preparing SiNW building blocks that switch on and off at lower voltages (*24*). Nevertheless, the present devices still exhibit the low static power dissipation expected of a complementary inverter-like structure; that is, the SiNW complementary device has a static dissipation of 0.5 to 5 nW in either high or low states, whereas a single SiNW device has a power dissipation 10^3 to 10^4 larger.

Our studies demonstrate a rational approach for building key nanoscale electronic devices from SiNWs that have controlled carrier type and concentration, and thus represent a step toward a "bottom-up" paradigm for electronics manufacturing. Although these studies have focused on the assembly and properties of single SiNW-based devices, combination of this approach with emerging methods for hierarchical assembly (*25, 26*) could enable parallel and scalable organization of complex electronic devices on a bench top.

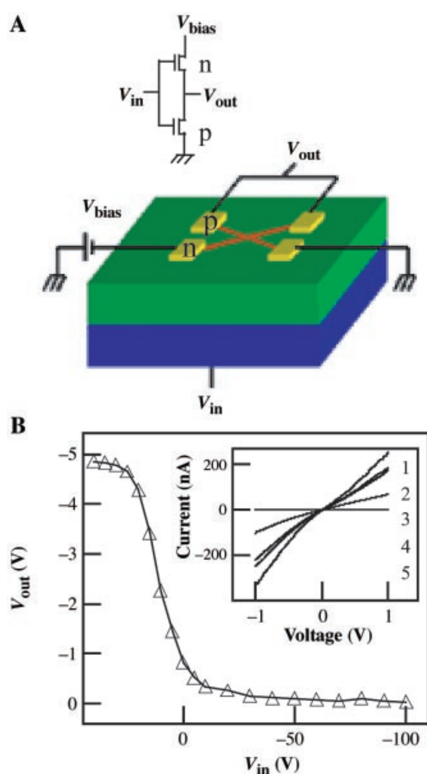

Fig. 3. SiNW complementary inverters. (**A**) Standard representation (*19*) of a complementary inverter formed using *n*- and *p*-type field-effect transistors (top) and a schematic of a similar structure assembled from *n*- and *p*-type SiNWs (bottom). In the NW device, one end of the *n*-type NW is biased at negative voltage and one end of the *p*-type NW is grounded. The back gate voltage is V_{in}, and the other ends of the *p*- and *n*-type NWs are connected as V_{out}. (**B**) V_{out} versus V_{in} for a *p-n* complementary inverter-like structure. The inset is the *I-V* curves of *p*-type NW in the inverter. Curves 1 to 5 correspond to *I-V* at back gate voltage –50, –30, –10, 0, and 10 V, respectively.

References and Notes

1. P. Peercy, *Nature* **406**, 1023 (2000).
2. G. Timp, *Nanotechnology* (Springer-Verlag, New York, 1999), pp. 161–206.
3. C. B. Murray, C. R. Kagan, M. G. Bawendi, *Science* **270**, 1335 (1995).
4. C. A. Mirkin, R. L. Letsinger, R. C. Mucic, J. J. Storhoff, *Nature* **382**, 607 (1996).
5. A. P. Alivisatos *et al.*, *Nature* **382**, 609 (1996).
6. J. R. Heath, P. J. Kuekes, G. S. Snider, R. S. Williams, *Science* **280**, 1716 (1998).
7. J. Hu, T. W. Odom, C. M. Lieber, *Acc. Chem. Res.* **32**, 435 (1999).
8. C. Dekker, *Phys. Today* **52**, 22 (May 1999).
9. S. J. Tans, R. M. Verschueren, C. Dekker, *Nature* **393**, 49 (1998).
10. R. Martel, T. Schmidt, H. R. Shea, T. Hertel, P. Avouris, *Appl. Phys. Lett.* **73**, 2447 (1998).
11. S. J. Tans *et al.*, *Nature* **386**, 474 (1997).
12. M. Bockrath *et al.*, *Science* **275**, 1922 (1997).
13. J. Hu, M. Ouyang, P. Yang, C. M. Lieber, *Nature* **399**, 48 (1999).
14. Z. Yao, H. W. C. Postma, L. Balents, C. Dekker, *Nature* **402**, 273 (1999)
15. M. S. Fuhrer *et al.*, *Science* **288**, 494 (2000).
16. Y. Cui, X. Duan, J. Hu, C. M. Lieber, *J. Phys. Chem. B* **104**, 5213 (2000).
17. The *p*- and *n*-type SiNWs were dispersed in acetone, and deposited sequentially onto an oxidized (600 nm SiO_2) Si substrate (1 to 10 ohm·cm) to form *p-n*, *p-p*, and *n-n* junctions. Aluminum (50 nm) gold (150 nm) contacts were deposited by thermal evaporation (*16*) and used without further annealing.
18. Plots of conductance (d*I*/d*V*) versus voltage for single *p*- and *n*-type wires in *p-n* (Fig. 1B) and other junctions show voltage-independent behavior or small drops in conductance around $V = 0$; no gaps are observed. These data (and corresponding *I-V* results) demonstrate that the metal-SiNW contacts do not exhibit a significant Schottky barrier (are ohmic in many cases), and thus that the observed nonlinearities reflect transport through the NW-NW junctions.
19. S. M. Sze, *Physics of Semiconductor Devices* (Wiley, New York, 1981).
20. H. C. Card, E. H. Rhoderick, *J. Phys. D Appl. Phys.* **4**, 1602 (1971).
21. TEM studies show that the SiNWs have an amorphous oxide coating 1 to 2 nm in thickness and sometimes less than 1 nm in thickness (Y. Cui, L. Lauhon, C. M. Lieber, unpublished results).
22. The n^+-*p*-*n* bipolar transistors were fabricated by deposition and manipulation. First, *p*-type SiNWs were deposited from solution onto the substrate. Then the n^+- and *n*-type SiNWs were attached to etched metal tips and assembled across the *p*-type SiNW using micromanipulators in an optical microscope.
23. The small increase in collector current (Fig. 2C, II) could be due to a decrease in the effective base width and/or increasing leakage current as the C-B voltage is increased (*19*). When the C-B voltage is <0, the bipolar transistor is in the saturation mode (Fig. 2C, regime I) with both E-B and C-B junctions forward-biased. When both junctions are forward-biased, the collector current due to emitter injection is compensated by the C-B injected current.
24. Recent gate-dependent transport measurements on individual SiNWs with ~10 nm diameters showed an on/off ratio larger than 10^4 with a gate voltage of 5 V. See supplementary data (www.sciencemag.org/cgi/content/full/291/5505/851/DC1).
25. C. A. Mirkin, *Inorg. Chem.* **39**, 2258 (2000).
26. The use of fluidics and chemical patterning has been shown to be a powerful technique organizing nanowires into parallel, crossed, and more complex arrays over large length scales. Because assembly can be carried out in a layer-by-layer fashion, it is possible to create homo- and heterojunctions [Y. Huang, X. Duan, Q. Wei, C. M. Lieber, *Science* **291**, 630 (2001)].
27. We thank X. Duan, M. Gudiksen, J.-L. Huang, K. Kim, L. Lauhon, T. Oosterkamp, M. Ouyang, H. Park, and J. Wang for helpful discussion. C.M.L. acknowledges support of this work by the Office of Naval Research and Defense Advanced Projects Research Agency.

10 October 2000; accepted 5 January 2001